

Dynamic behavior and prevention of the damage of material  
of the massive hammer of the scrap shredding machine

*Original*

Dynamic behavior and prevention of the damage of material  
of the massive hammer of the scrap shredding machine / Brusa, Eugenio; S., Morsut; Bosso, Nicola. - In: MECCANICA.  
- ISSN 0025-6455. - ELETTRONICO. - (2014), pp. 575-586. [10.1007/s11012-013-9812-x]

*Availability:*

This version is available at: 11583/2513722 since:

*Publisher:*

Springer

*Published*

DOI:10.1007/s11012-013-9812-x

*Terms of use:*

This article is made available under terms and conditions as specified in the corresponding bibliographic description in the repository

*Publisher copyright*

(Article begins on next page)

# Dynamic behavior and prevention of the damage of material of the massive hammer of the scrap shredding machine

Eugenio Brusa · Stefano Morsut · Nicola Bosso

**Abstract** Shredders are used for comminuting the metallic scrap fed to the electric arc furnace and consist of a set of hammers connected to a main rotor, whose rotation converts the kinetic energy into a strong impact. Design of the hammer is still based on some daily practice, but often it looks insufficient to predict the effects of wear and the cracks monitored in service. To reduce costs and improve the product quality manufacturers of shredders urgently need for a design tool suitable to predict the hammer dynamic behavior, the damage of material and to locate the stress concentration. Unfortunately no comprehensive design approach was yet proposed in the literature. This paper investigates the behavior of an industrial prototype of shredder to develop such as design tool. A first rotor-dynamic analysis was combined with a numerical investigation, performed through the Multi

Body Dynamics and Finite Element Method, respectively. Results were then compared to some experimental evidences. Damage effects were tentatively related to some design parameters, the material properties and the loading conditions of the hammer. Results were used to increase the performance of a new shredder hammer being designed by refining the cutting edge profile and by selecting a different material.

**Keywords** Shredder hammer · Multi-body dynamics · Finite Element Method · Stress analysis · Steelmaking equipment · Mechanical design

## Symbols

$F_c$  centrifugal force  
 $F_i$  impact force  
 $K_{PS}$  ratio between the action applied to the pin and to the scrap  
 $K_W$  ratio between the action applied to the pin when cutting edge is new and in case of worn profile  
 $M_i$  impact moment  
 $R$  distance of the impact point from the disc centre  
 $V$  impact speed  
 $l$  length of the rotating pendulum  
 $r$  radius of the rotor disc  
 $\Omega$  angular speed of the disc rotor  
 $\alpha$  inclination of the anvil plane; absolute angle of rotation of the hammer symmetry axis in the fixed reference frame  
 $\beta$  angular position of the impact point in the fixed reference frame

---

E. Brusa (✉) · N. Bosso

Department of Mechanical and Aerospace Engineering,  
 Politecnico di Torino, Corso Duca degli Abruzzi,  
 24-10129

Torino, Italy

e-mail: eugenio.brusa@polito.it

url: <http://www.dimeas.polito.it>

N. Bosso

e-mail: nicola.bosso@polito.it

S. Morsut

R&D Department, Danieli SpA, Via Nazionale, 33100

Buttrio (Udine), Italy

e-mail: s.morsut@danieli.it

url: <http://www.danieli.com>

$\gamma$	angular position of the impact point on the inner surface of the hammer hole
$\delta$	angle between the impact force and the hammer axis
$\zeta$	angular position of the hammer axis
$\theta$	in-plane rotation of the disc pendulum frequency of the pendulum
$\lambda$	
$\phi$	out-of-plane rotation of the disc pendulum

## 1 Introduction

Shredder hammers are used to reduce the size of the ferrous scrap fed into the electric arc furnace [1]. Big rotors are equipped with several hammers [2], whose impact against the scrap provides the fragmentation [3] and the comminution [4] of dismissed mechanical parts. Some typical damages occur during the life of the shredder hammer and affect its dynamic response [5]. A severe wear of material is observed on the cutting edge and on the hammer surface, where it is in contact with the pin of the rotor disc. Some cracks appear on the pin-to-hole contact surface together with a thermo-mechanical alteration of the material properties. Effective design rules to predict those damages are not yet available, although some approaches were proposed [6]. An urgent need of the shredder manufacturer consists of a design tool, being suitable to predict the hammer dynamic behavior, the impact actions, the stress distribution and the location of cracks. A preliminary investigation was therefore performed to define the critical points of the hammer and to optimize its design. Typical failures were first detected on a monitored shredder machine. Modeling activity was then developed to predict the dynamic behavior of each hammer. Numerical models were built into a Multi Body Dynamics, to evaluate the impact actions

and the rigid body motions, then into a Finite Element code, to perform the stress analysis, locating the crack occurrence and predict the plasticity region around the hole. This investigation was performed by considering the role of the angular speed, the friction among the materials, the gap between the pin and the hammer and of the shape of the cutting edge. A preliminary correlation among the damages and some design parameters of the hammer was found and used to improve the shape of the cutting edge. Unfortunately, an exhaustive experimental validation of the numerical models is currently impossible because of the inaccessibility of the shredder machine in operation, mainly due to the dangerous projections of material.

## 2 System description and experimental evidences of damage

The rotor bears a set of discs, equipped with several hammers, connected by hinges. Each hammer freely rotates about the pin axis. A clearance is there provided and usually spans from 10 to 20 mm, being larger in the worn shape. Rotation, performed at 500–750 rpm, causes a strong impact of each hammer against the scrap, supported by the anvil (Fig. 1). A gap is left between the hammer and the anvil, being usually set up to 40–100 mm. Scrap continuously drops out of the feeding roller at a speed of 0.1–0.4 m/s towards the anvil and includes ferrous parts with a size of about 200 mm<sup>3</sup>.

A preliminary analysis of damage, being performed upon an operating shredder, allowed observing that a severe wear applies to the hammer material at the hole as pictures of Fig. 2 describe and changes the shape of the cutting edge, because of the repetitive impact

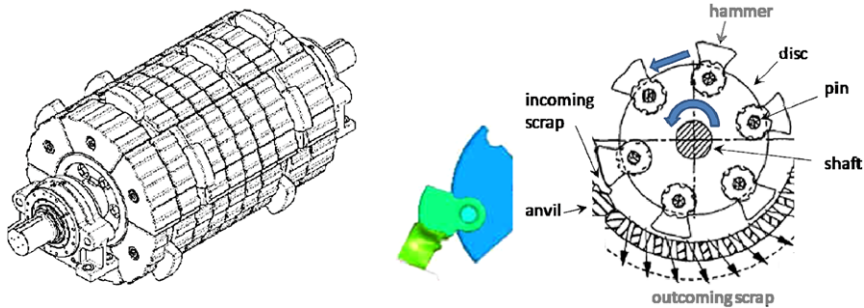


**Fig. 1** Sketch of the shredder rotor and pictorial example of its operation

against the scrap, as shown in Fig. 3, where some worn shapes of the hammer are depicted.

This effect is due to the continuous friction between the hammer and the scrap, but it depends on the rotor spin speed and the mass distribution in the hammer. Some cracks occur on the inner surface of the hammer hole, being located at the left quadrant of the upper half-circumference. According to the manufacturer origin of the cracks is uncertain, being potentially caused by the impulsive action of impact, fatigue or thermo-mechanical fatigue [7]. An evident out of

roundness of the hole is observed. Magnitude of those damages depends on the frequency of the whirling motions of the hammer-rotor system. Unfortunately, no information about forces and moments acting on the system were available nor measured values of temperature. Therefore numerical investigations were aimed to evaluate first the actions applied to the hammer to perform then the complete analysis of its dynamic behavior.

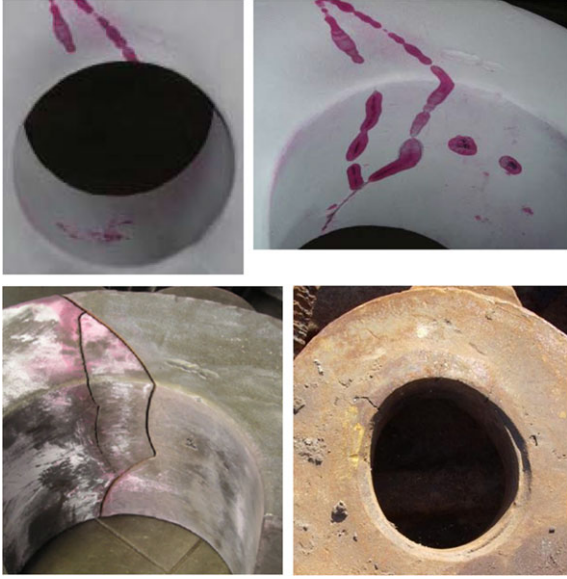


**Fig. 2** Pictures of some typical damages detected in service on the shredder hammers

### 3 Preliminary modeling activity

To proceed straight in investigating the dynamic behavior of the hammer, some values of angular speed and of gap between the hammer and the pin were considered and three geometries of the hammer were analyzed. The behavior of the original shape, as it looks when the shredder is just manufactured, was compared to that of two worn layouts, depicted in Fig. 3. The first is corresponding to the worn geometry after a first pe-riod of service, during which the cutting edge is made smoother by the repetitive impact. The hammer is then usually rotated, during a stop of the shredder machine, to use the rear part of the cutting edge. Therefore the second layout looks like the hammer appears after a complete wear of the material. The performance of steels FeE420 and FeP04, respectively, was investi-gated.

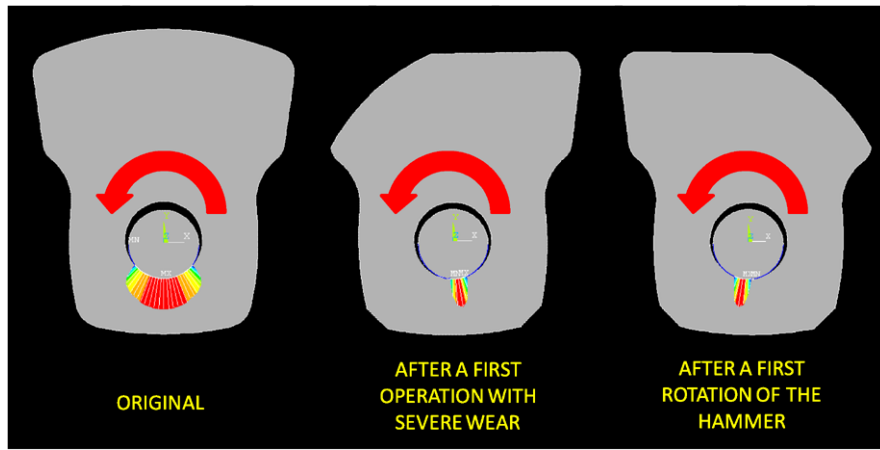


**Fig. 3** The three configurations of the shredder hammer analyzed: original, worn, worn and rotated after maintenance operation

### 3.1 Impact models

Constraints in measuring all the actions applied to the system in operating conditions required a preliminary study of the order of magnitude of the impact excitation. A centrifugal action of 500–1000 kN is applied to the hammer mass of about 200 kg, for a given distance between the pin and the centre of the disc of  $r = 730$  mm, while the centre of mass of the hammer is located about at 850 mm. Impact force depends on the nature and the size of the scrap. It can be 5000–8000 kN, if a perfect plastic collision is assumed, in case of ‘soft scrap’, while it reaches 18000–20000 kN in case of lateral collision on ‘elastic-plastic scrap’ body. Very seldom it grows up to 50000–150000 kN, if the scrap is assumed to be perfectly rigid and collision totally elastic. Manufacturer made a screening of the scrap usually fed into the shredder and defined a reference configuration. A tubular structure of steel with square cross section, wall thickness spanning from 10 to 30 mm, variable length and opening size of about 200 mm was used to compute approximately the order of magnitude of impact, according to Jones [8] and by including both the cases of impact and buckling. Three levels of impact forces were finally identified as 1500 kN (soft scrap, easy crash), 5000 kN (intermediate scrap) and 20000 kN (hard scrap accidentally present in feeding flow). These values were assumed as a reference to perform the numerical investigations.

### 3.2 Dynamics of the hammer pendulum rotor

If the hammer is seen as a rotating pendulum the main effects of unbalance can be predicted [9]. In Fig. 4,  $OA = r$ ,  $AB = l$  and  $\Omega$  describes the angular speed about the rotor axis, while angle  $\theta$  is used to describe the oscillation of pendulum AB in the disc plane, being angle  $\phi$  the rotation out of plane.

The kinetic energy associated to the mass of the rotating pendulum, located at B, can be described as:

$$T = \frac{1}{2}m|V_B|^2 = \frac{1}{2}m[r^2\Omega^2 + l^2\dot{\phi}^2 + l^2(\Omega + \dot{\theta})^2\cos^2\phi - 2\Omega r l \dot{\phi} \sin\phi \sin\theta + 2\Omega r l (\Omega + \dot{\theta}) \cos\phi \cos\theta] \quad (1)$$

where  $V_B$  is the speed of point B.

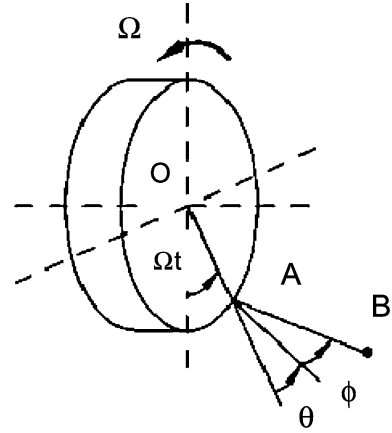


Fig. 4 Sketch of the equivalent rotating pendulum

Dynamic equilibrium equations of motion of point B are found by means of the Lagrangian approach:

$$\frac{d}{dt}\left(\frac{\partial T}{\partial \dot{\theta}}\right) - \frac{\partial T}{\partial \theta} = 0 \quad \text{and} \quad \frac{d}{dt}\left(\frac{\partial T}{\partial \dot{\phi}}\right) - \frac{\partial T}{\partial \phi} = 0$$

(a)  $l\ddot{\theta}\cos^2\phi - 2l(\Omega + \dot{\theta})\dot{\phi}\cos\phi\sin\phi + r\Omega^2\cos\phi\sin\theta = 0$

(b)  $l\ddot{\phi} + l(\Omega + \dot{\theta})^2\cos\phi\sin\phi + r\Omega^2\sin\phi\cos\theta = 0$

If the system is linearized about the equilibrium condition, the above equations look simplified as follows:

$$(a) \quad l\ddot{\theta} + r\Omega^2\theta = 0$$

$$(b) \quad l\ddot{\phi} + (r + l)\Omega^2\phi = 0 \quad (3)$$

Those equations allow computing the two typical frequencies of the rotating pendulum:

$$\lambda_a = \Omega\sqrt{r/l} = 2.44 \cdot \Omega;$$

$$\lambda_b = \Omega\sqrt{1 + r/l} = 2.64 \cdot \Omega; \quad (4)$$

where  $\lambda_a$  is corresponding to the in-plane motion and  $\lambda_b$  to the out-of-plane motion, respectively. If numerical values of radius  $r$  and length  $l$  are substituted inside those solutions, it can be remarked that the corresponding frequencies are quite close each other and included in the range of spin speed from 2 to 3 times the synchronous excitation,  $\Omega$ . Operation of the shredding machine shows that a wide range of frequen-

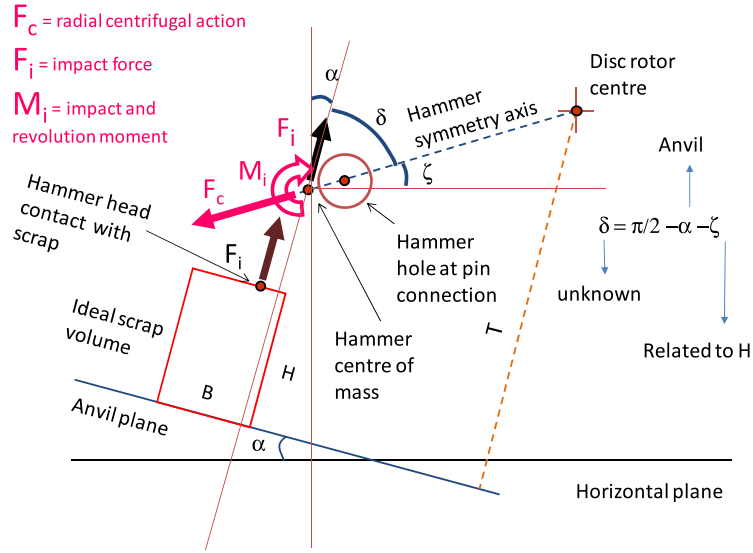


Fig. 5 Sketch of the hammer configuration when impact against the scrap body occurs

cies excite the dynamic response of the rotating system. The largest effects are observed between  $0.5\Omega$  through  $3\Omega$ , because of the simultaneous action of several hammers distributed along the rotor axis and of some nonlinearity present in the system behavior. Those frequencies are included into that range and the related motions look fairly excited, in absence of friction or damping. These excitations do not superpose directly on the synchronous one ( $\lambda = \Omega$ ) and to the weight effect ( $\lambda = 2\Omega$ ), but they look fairly active as well as the following MBD simulations revealed. Moreover, moments opposed by the friction to the motions related to the vibration modes described by solutions in Eq. (4) may reduce their amplitude, but simultaneously cause a local dissipation, with a growing up of the temperature, if the residual displacement is sufficiently large. The severity of this phenomenon depends on the coefficient of friction between the materials. Increasing the values of those critical speeds by a larger ratio  $r/l$  looks in contrast with the requirement of compactness of the rotor system.

### 3.3 Properties of the materials

To perform the stress analysis of the hammer material into the numerical code it is required inputting the characteristic curve in terms of stress vs. strain, for a given strain rate. For the materials selected by the manufacturer three were the available curves, obtained by the tensile test machine for a strain rate of

$0.0015 \text{ s}^{-1}$ ,  $3 \cdot 10^{-1} \text{ s}^{-1}$  and  $500 \text{ s}^{-1}$ . Prediction of the strain rate does not look straightforward because the strain tensor contains up to six different components, in case of isotropic material. In this case it was simpler defining a figure of strain rate for the material of the scrap material, provided that a reference geometry was previously defined and a main component of strain defined. Further more difficult is the investigation in case of the hammer. As Fig. 5 shows at least the speed reached by the hammer at the impact against the scrap was first investigated:

$$V = R\Omega \sin(\delta) \quad (5)$$

being  $V$  the tangential speed reached by the hammer during its rotation,  $\Omega$  the angular speed,  $\delta$  the orientation angle of impact force with respect to the symmetry axis of the hammer, and  $R$  the distance between the cutting edge and the rotor axis.

If the range of the scrap height is 100–500 mm and dimensions of the hammer are those of the monitored shredder, the speed at the impact is 50–80 m/s. For the reference shape of the scrap, which has been assumed to be tubular with square cross section, under the assumptions proposed by Jones [8] the strain rate of the maximum strain, acting along the direction of the sides of the cross section during the compression induced by the impact force, was computed and values were found spanning from 40 to  $70 \text{ s}^{-1}$ . Finite element code allowed analyzing the strain distribution

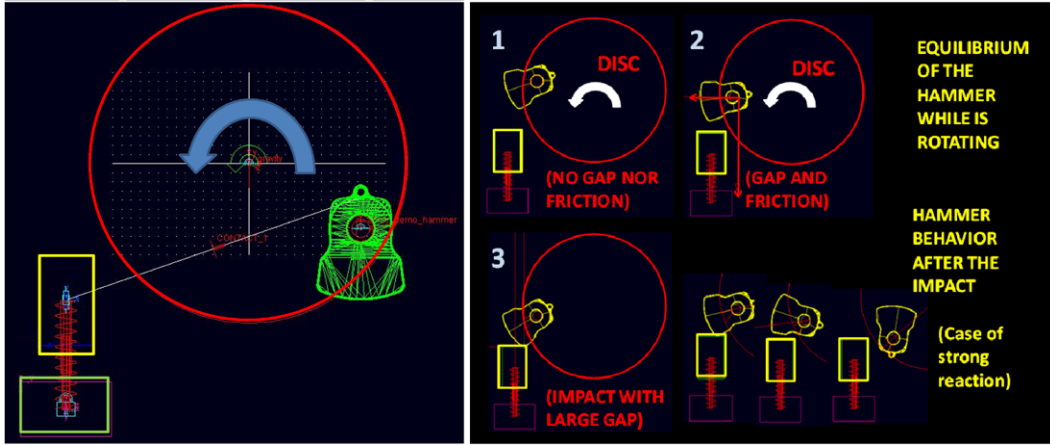


**Fig. 6** Sketch of the MBD model of the shredder hammer and of some configurations in rotation

in the case of the hammer, thus demonstrating that many strain components are active at the impact, but the most important is that along the direction of the impact force in both the locations where contact occurs, i.e. between the cutting edge and the scrap and between the hammer hole and the pin. Those values were computed through the finite element method during the advanced step of this investigation. It was assumed that among the three stress-vs-strain curves of materials proposed those obtained for  $30 \text{ s}^{-1}$  could be the most close to the actual dynamic behavior of the system, at least preliminarily.

In addition for those operating conditions it can be remarked that yielding of the FeE420 steel occurs at the 67 % of its tensile strength, while the FeP04 steel exhibits a tensile strength 2.3 times larger and its elastic-plastic behaviour starts at the 28 % of it. These properties motivate the different dimensions of the plastic region numerically predicted by the FEM code, around the hammer hole during the impact.

## 4 Multi-body dynamic analysis

### 4.1 Model

Three values of impact force (1.5, 5, 20 MN) were initially considered to run the Multi-Body Dynamics code. A disc with a single hammer was analysed (Fig. 6). In the MBD model the scrap looks modelled as a rigid body supported by a spring-damper compliant system. It moves along the horizontal direction

towards the mill, at a constant speed, while displacement is inhibited along the vertical direction. When impact occurs spring is compressed and comminution is simulated. Hammer is a rigid body connected to the disc rotor, which rotates at constant spin speed. Gap between the hammer and the pin is set up at each simulation.

Friction forces are figured between the hammer and both the scrap and the pin, respectively. Friction coefficients were set at 0.5 (static) and 0.3 (dynamic), according to the properties of the tested materials. Simulation was performed by accelerating the disc from zero up to the defined angular velocity. After few rotations hammer reaches its equilibrium under the centrifugal action. Impact occurs while the scrap is moving towards the mill. Equations of motion of are solved in the time domain.

A preliminary identification of values of the equivalent stiffness and damping coefficients of the spring-damper system was required. They were found by imposing the values of impact force and strain rate previously found. Impact angle of the hammer, direction, versus and magnitude of the impact forces applied to the scrap and to the pin, respectively, were computed. Location of the contact point on the inner surface of the hammer hole was evenly detected.

### 4.2 Numerical results and discussion

Many were the relevant results of this first numerical investigation, being herein briefly summarized. Amplitude of the impact force on the scrap does not only



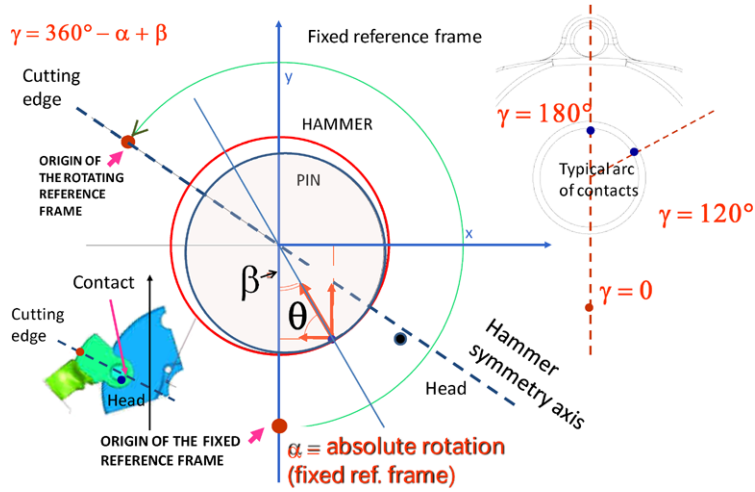


**Fig. 7** Reference frames and angles used to describe the dynamic impact on the pin

affect the magnitude of contact force on the pin but even the dynamic response of hammer in rotation. Low impact force and appreciable friction make the hammer moderately rotating about the pin axis after the impact, contact forces are remarkable, being applied to a limited portion of the hole circumference. When the impact force is larger, contact occurs along a longer arc, leading to a smaller contact force. Unfortunately, it looked impossible finding a ratio between the value of the impact force applied by the hammer on the scrap and on the pin, respectively, for different spin speeds. Distance of the centre of mass of the hammer from the rotor centre is crucial. If it is longer, rotation about the pin is larger and dynamic behaviour of the hammer seems fairly irregular.

The worn layouts give a smaller impact effect and even the kinetic energy drop is smaller. Contact between the hammer and the pin is located at the upper circumference, between angle  $\gamma = 120^\circ$  and  $180^\circ$ , being this angle defined as in Fig. 7.

This location of the contact point precisely corresponds to the position of the cracks detected in service (Fig. 2). Contact force applied on the pin is usually larger than on the scrap. As Fig. 8 shows after the first peak due to the impact, a series of repeated actions follow, but if the impact force is larger, the following peaks are lower and excitation appears more uniform over time.

In the worn layout contact between the pin and the hammer occurs at  $\gamma = 180^\circ$  and after the impact, hammer seems to be borne by the scrap at the cutting edge,

while the disc is rotating. A larger gap between the anvil and the hammer could be useful to have smaller excitations in this case (Fig. 9). Nevertheless, it is worthy noticing that for an impact force of 1.5 MN, contact force is lower than in case of 5 MN, but reduction is less than it was expected. A small gap between hammer and pin helps in having smaller impact actions and stress concentration around the hammer hole.

Time to reach the maximum value of impact force significantly increases at a lower spin speed of the rotor, repetition of hits after impact is fairly long, although their amplitude is less than for higher spin speeds. Wear of material is less severe, in terms of applied load, but more effective in terms of persistence on a small region of the hammer.

A summary of the numerical results computed by the MBD code is shown in Table 1. Factor  $K_{PS}$  describes the ratio between the force applied to the pin and the scrap, respectively, while  $K_W$  is the ratio between the force acting on the pin, in case of the original layout and for the worn ones.

## 5 Finite element analysis

### 5.1 Modeling

FEM analysis looked rather difficult because of several computational issues and some nonlinearities. A first comparison between a three dimensional model of the



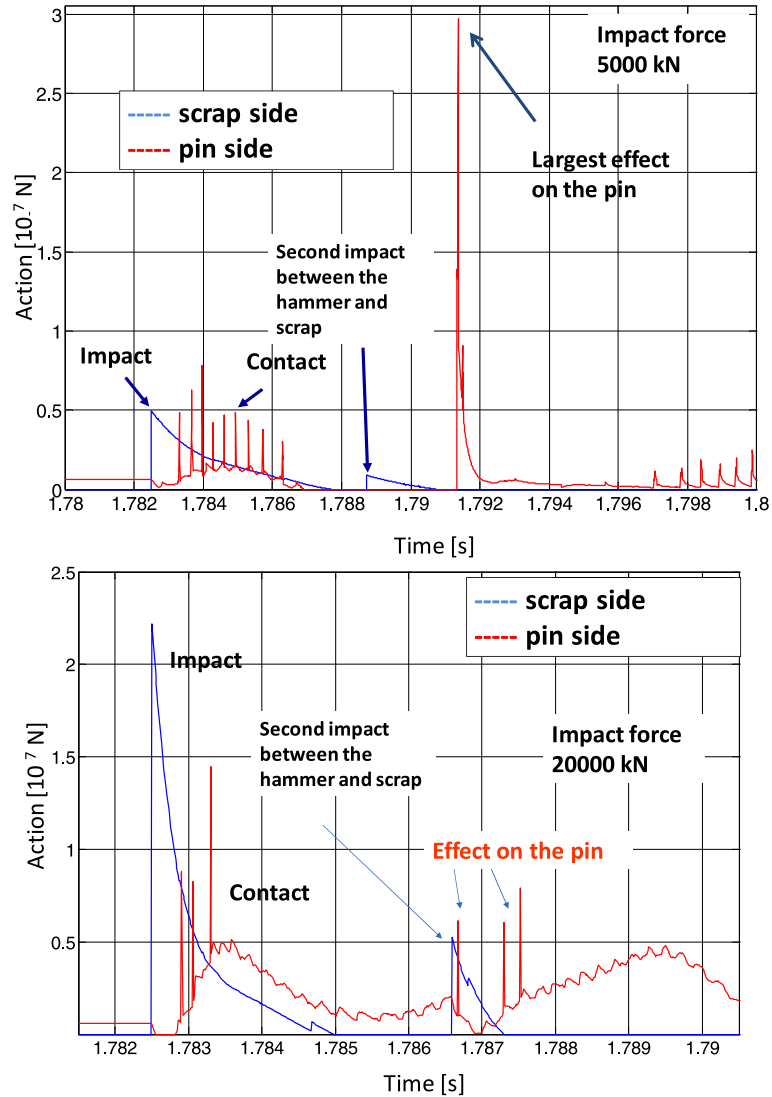


**Fig. 8** Force applied to the hammer, in presence of clearance, for an impact force on the cutting edge of 5000 kN and 20000 kN, respectively

hammer and a two dimensional one allowed realizing that the latter could be sufficient to investigate where the critical stress is located and to evaluate its magnitude. Three dimensional models show severe problems of numerical convergence and require a huge computational effort, caused by the large value of the load here applied. In the plane model the assumption of plane state of stress with finite thickness can be made. Case of the pure rotation of the hammer without impact force was compared to the loading condition at the impact. Nonlinear solution took simultaneously into account the effects of nonlinear stress-strain curve

of each material and of contact. Curves of materials were directly provided by Danieli® as a function of the strain rate and inputted into the code. Loading condition at impact was identified first through the MBD and applied to FEM model. Nonlinear solution was computed by simulating the last approach motion of the hammer towards the pin surface, i.e. by focusing on few seconds before and after the impact. All the inertial loads were introduced and the instantaneous condition for contact was found out. Pin was assumed constrained, while the hammer was reaching the equilibrium condition. This approach allowed avoiding to

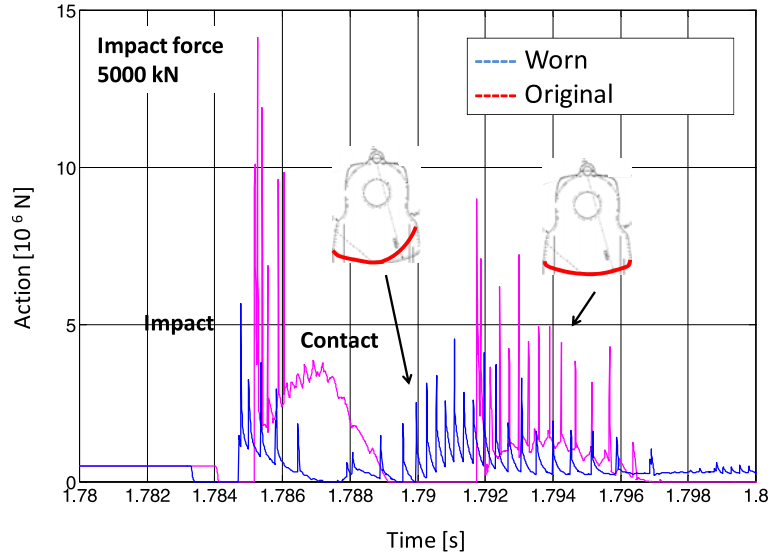


**Fig. 9** Force applied to the pin, for a gap of 15 mm, under an impact force on the cutting edge of 5000 kN

**Table 1** Loads due to the impact between the hammer and pin

[MN]	Original	Worn	Rotated
Action on scrap	5	5	3.8
	20	18	20
	80	82	80
$K_{PS}$ (Fpin/Fscrap)	1.6	2.8	1.6
	0.7	2.1	0.6
	0.3	0.36	0.35
$K_W$	1	1.75	0.75
(Fpin, worn/	1	2.7	0.86
Fpin, no wear)	1	1.2	1.12

run an explicit solution. Manufacturer considered this task out of the goals of this analysis. Nevertheless this model looked sufficient to detect the stress distribution and to compare some proposed layouts of the hammer. An absolute detection of stress could be only possible after a calibration of the numerical model on some experimental test, currently not yet available. Pure rotation condition, without impact, was investigated to compute the mean stress acting on the hammer. Impact was then analysed. In this case the maximum value of impact force allowing the FEM code converging was reached, i.e. for each configuration analysed the yield-

ing of material was found and the plastic region was localized.

## 5.2 Results and discussion

Some examples of numerical results of the stress analysis are shown in Figs. 10 and 11, being expressed in a non dimensional format with respect to the yield-ing stress,  $\sigma_Y$ . Maximum principal stress ( $\sigma_1$ ) and the equivalent value computed according to Von Mises ( $\sigma_{eq}$ ) are plotted. On the left side of each figure the case of pure rotation is described, while on the right one the maximum impact load numerically investigated is shown.

Some localized peaks of stress, inducing the plastic strain, may be reached in pure rotation just around the first contact point. Centrifugal actions due to the spin speed gradually modify the shape of the hammer hole, which tends to become oval. Pin is a critical component. Stress distribution shows a gradient across the section and peaks are fairly large. When impact surface between scrap and hammer is larger, as in the worn geometry, stress around the hole is lower and the maximum impact load allowing the numerical convergence is bigger. For a given value of impact force, plastic region looks fairly different, if the pressure applied by the scrap on the cutting edge is either distributed over a large portion of the profile or concentrated around its corner. The maximum load appli-

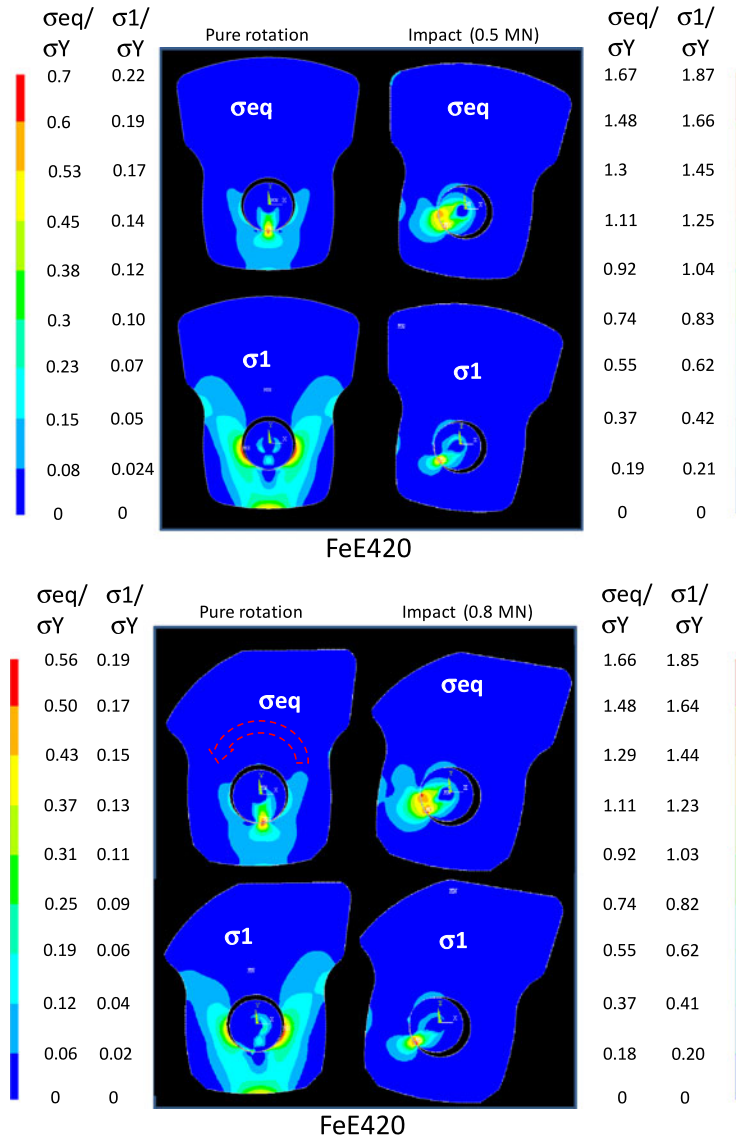


**Fig. 10** FEM stress analysis, material FeE420, original and worn shapes, 600 rpm

cable seems larger, because of rotation of the hammer is smaller.

Plastic region is smaller for the FeP04 steel. This difference is related to the look of the stress vs. strain curve. FeE420 follows a linear elastic behaviour, achieves the yielding stress, then its curve slowly grows up to the tensile strength. FeP04 achieves the yielding stress, then tensile strength is reached through a nearly straight line, whose slope is fairly lower than in case of the linear elastic behaviour, thus providing a better performance.

## 6 Discussion and design criteria

As the numerical investigation shows the superposition of a number of effects in this system makes practically impossible an intuitive prediction of its dynamic behaviour. Nevertheless some motivations to the damages monitored were found.

Since the beginning of the shredder operation the rotation induces a remarkable wear effect, due to the rotating pendulum motion of the hammer about the pin. Frequency of this phenomenon has to be distinguished as much as possible from the synchronous

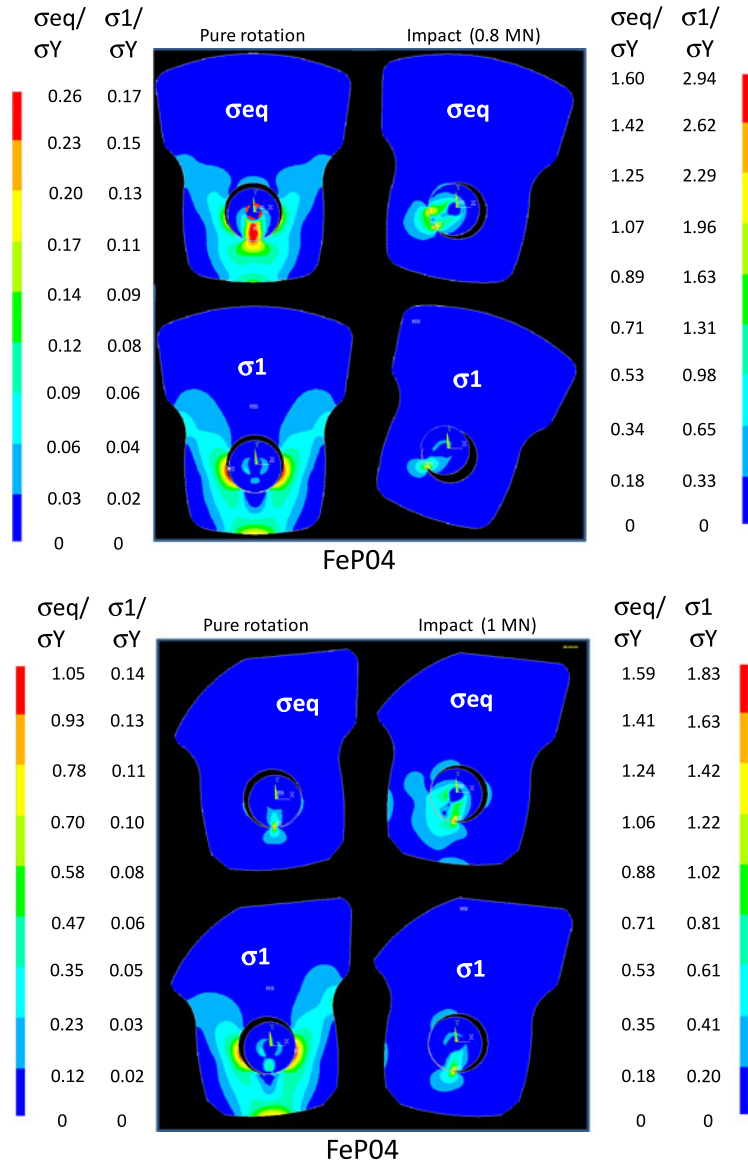


**Fig. 11** FEM stress analysis, material FeP04, original and worn shapes, 600 rpm

excitation, through a suitable proportioning of the length of the hammer. Centrifugation applies a fairly high level of stress and the hammer hole tends to become oval. Gap between pin and hammer gradually increases. All dynamic effects are magnified and look more nonlinear. This gap should be kept as small as possible or designer can resort to the so-called 'integral solution' [10], where each hammer is part of the disc rotor. If the angular speed is slow wear works slowly, but the impact against the scrap is less effective. At each impact a first strong collision occurs,

then a sequence of smaller impacts follows. Their frequency is almost constant and amplitude is regular. Pendulum motion is easily damped, shaping effect on the hammer hole is reduced, but if the angular speed is too low the rotation of the hammer about the pin axis may compromise the process. In present case the range of the spin speed defined was found compatible with the needs.

Identifying the actual amplitude of the impact load is really difficult. An experimental monitoring looks practically impossible. Heavier impact forces do not

have necessarily a worst effect on the hammer and a sharper nose on the cutting edge may be useful. A stronger impact excites more the pin, but the hammer performs a larger rotation about the pin. The arc of contact explored in the hammer inner surface is larger and stress is lower. Yielding can be reached at least locally if the impact action is about 1000–3000 kN. This issue makes important the plastic behaviour of material, i.e. the look of its stress-vs-strain curve, for a given strain rate. It is worthy noticing that wear of the cutting edge is correlated to the material damage at the hammer hole. If cutting edge profile is smooth or worn, shredding pressure applies to a larger surface and contact between hammer and scrap is longer. After the main impact the hammer is almost borne by the scrap and a sequence of hits can be observed, being even larger than the first impact. Nevertheless, arc of contact between hammer and pin is larger and stress concentration is lower. These results suggest to introduce an hub between the hammer and the pin to reduce the effect of the impulsive loads.

Angular position of the first contact was localised between  $120^\circ$  and  $180^\circ$  in the reference frame of the hammer, being agreeing with the experimental evidences of Fig. 1. When the hammer undergoes a pure centrifugation at constant speed,  $\gamma = 180^\circ$  is the location of the peak of stress. In case of impact and of a sharper cutting edge, like in the original layout, angle is about  $\gamma = 120^\circ$ – $140^\circ$ . These values are compatible with the location of cracks detected in service, thus indicating that damage is mainly due to impact more than to fatigue. Thermo-mechanical fatigue may have a role, if temperature rises up because of the friction between the two surfaces. Even from this point of view the FeP04 steel looks more suitable, because it can bear an higher impact force, plastic region is smaller and its plastic behaviour can be compatible with a longer strength against low cycle thermo-mechanical fatigue.

## 7 Conclusion

A preliminary analysis of the dynamic behaviour of a shredder hammer was performed, in spite of lack of models in the literature. A combined approach based on both analytical and numerical methods was followed. A first analysis of the pendulum motion in rotation allowed realizing that critical speeds are quite

close to the synchronous excitation. The Multi Body Dynamics model identified the impact forces applied to the hammer and the pin respectively, while the Finite Element Method computed the stress distribution. Loads are fairly large, up to 1–5 MN and stress concentration occurs around the contact between the hammer and the pin. In case of impact force equal to 0.5–1 MN the strength of material is reached, at least on a small area of the hammer. The performance of some materials was investigated. Impact effect is larger when the hammer is new and its cutting edge is somehow sharper. In this configuration a main risk is cracking, at the inner surface of the hammer hole. Wear is very effective on the cutting edge, because of the shredding process but also of the hammer whirling. When the cutting edge is smoother, scrap bears the hammer for a longer time after the impact and hits the hammer head repetitively. In practice adding mass to the hammer head decreases the frequency of the pendulum rotor and increases the impact action on the hammer hole material. Shaping the impact nose of the head as a sharper tool may be useful to increase the comminution, without changing the distributed inertia. To effectively decrease the occurrence of early cracks in operation an inner hub seems required, although manufacturing costs of the shredder may increase.

## References

1. Aboussouan L et al (1999) Steel scrap fragmentation by shredders. *Powder Technol* 105:288–294
2. Sander S, Schubert G (2003) Size reduction of metals by means of swing hammer shredders. *Chem Eng Technol* 26(4):409–415
3. Russo P et al (2004) Mechanical and metallurgical study of the fragmentation of end-of-life goods in a scrap shredder. *Int J Miner Process* 74S:S395–S403
4. Sander S et al (2004) The fundamentals of the comminution of metals in shredders of the swing-hammer type. *Int J Miner Process* 74:385–393
5. Major A (1983) Dynamics in civil engineering: analysis and design. Akadémiai Kiadó, Budapest
6. Kosse V, Mathew J (2000) Design of hammer mills for optimum performance. *Proc Inst Mech Eng, Part C, J Mech Eng Sci* 215:87–94
7. Manson SS (1966) Thermal stress and low-cycle fatigue. McGraw-Hill, New York
8. Jones N (1997) Structural impact. Cambridge University Press, Cambridge
9. Genta G (2005) Dynamics of rotating systems. Springer, New York
10. Newell S (2007) Problem solving for shredders. The Shredder Company, LLC